



Facile microwave-assisted synthesis of monodispersed ball-like Ag@AgBr photocatalyst with high activity and durability

Xiang Xu^a, Xiaoping Shen^{a,*}, Hu Zhou^b, Dezhou Qiu^a, Guoxing Zhu^a, Kangmin Chen^c

^a School of Chemistry and Chemical Engineering, Jiangsu University, Zhenjiang 212013, PR China

^b School of Materials Science and Engineering, Jiangsu University of Science and Technology, Zhenjiang, 212003, PR China

^c School of Materials Science and Engineering, Jiangsu University, Zhenjiang 212013, PR China

ARTICLE INFO

Article history:

Received 1 December 2012

Received in revised form 27 January 2013

Accepted 28 January 2013

Available online xxx

Keywords:

Nanoparticles

Photocatalysis

Silver

Silver bromide

Microwave

ABSTRACT

We reported a rapid one-step microwave-assisted approach to synthesize a plasmonic photocatalyst of ball-like AgBr nanoparticles (*ca.* 290 nm in average diameter) with a small amount of metal Ag anchored on the surface. The obtained Ag@AgBr nanocomposites were characterized by means of X-ray diffraction, scanning electron microscopy, Transmission electron microscopy, energy dispersive X-ray spectroscopy, X-ray photoelectron spectroscopy and UV-visible diffuse reflectance spectroscopy. The shape, size, and compositions of the Ag@AgBr photocatalysts could be controlled by tuning the microwave irradiation time and the concentrations of polyvinylpyrrolidone (PVP) in the reaction solution. The as-prepared Ag@AgBr plasmonic photocatalysts show excellent visible-light photocatalytic performance and good reusability for decomposing organic pollutant of Rhodamine B (RhB) due to the surface plasmon resonance (SPR) effect of Ag nanoparticles. Meanwhile, the possible degradation pathways of RhB and a mechanism of the plasmonic photocatalytic process were also proposed.

© 2013 Elsevier B.V. All rights reserved.

1. Introduction

During the past decades, semiconductor photocatalysts based on harnessing and converting solar energy into chemical energy have attracted increasing attention because of their applications in solving the energy crisis and environmental pollution problems [1–6]. Typical example, TiO₂, is the most popular photocatalyst due to its peculiarities of chemical inertness, longterm stability against photocorrosion, abundance in nature, low cost, and non-toxicity [7–11]. However, the band gap of TiO₂ is larger than 3.0 eV, which means it can only absorb about 3–5% of sunlight in the ultraviolet region and the resultant low photocatalytic efficiency [12]. From the viewpoint of the efficient utilization of solar energy and higher photocatalytic efficiency, the development of visible-light-driven photocatalysts has recently become a very important topic of research. Consequently, anion-doping with C [13], N [14], S [15], and B [16] or cation-doping with transition metals [17] has been widely used to functionalize TiO₂ as a visible-light-driven photocatalysts. However, these doped TiO₂ materials show low absorption of visible-light; moreover, their photocatalytic activities are still very low due to massive charge carrier recombination. Therefore, it remains a great challenge to develop other effective visible-light-driven photocatalysts.

Noble metals (such as Ag and Au) nanoparticles have been extensively studied over the past decades due to their unique surface plasmon resonance (SPR) properties that can dramatically amplify the absorption of visible-light [18,19]. When noble metal nanoparticles are anchored on the surface of large-bandgap photocatalysts, they can act as a sensitizer to extend the light absorption region. For instance, Wang et al. have successfully synthesized Ag-loaded Bi₂WO₆ nanoarchitectures with enhanced photocatalytic activities [20]. Chen et al. have also reported plasmonic photocatalysts Au/ZrO₂ and Au/SiO₂ with high oxidation degradation efficiency for organic contaminants [21]. Recently, Huang and co-workers have developed a further type of plasmonic photocatalyst silver/silver halides (Ag@AgX; X = Cl, Br, I) by an ion-exchange reaction between aqueous solutions of Ag₂MoO₄ and HX followed by UV irradiation [22–26]. Sun and co-workers have reported a sunlight-driven AgCl/Ag photocatalyst by a direct reaction between AgNO₃ and NaCl under conventional oil-bath heating [27]. Since AgX can be *in situ* partially converted to plasmonic Ag nanoparticles, the interface between AgX and *in situ*-formed Ag is clean and well-defined, and the absorption coefficient of the resulting nanocomposites in the visible region can be significantly enhanced, which make Ag@AgX exhibit high photocatalytic activity and stability. Thus, the development of visible-light driven Ag@AgX photocatalysts has recently become a very important topic of research [28–33].

However, the reported Ag@AgX photocatalysts are often with large size and wide size distribution [22–26]. To the best of our

* Corresponding author. Tel.: +86 511 88791800; fax: +86 511 88791800.

E-mail address: xiaopingshen@163.com (X. Shen).

knowledge, there is no report on the monodispersed ball-like AgBr nanocrystals coupled with silver as plasmonic photocatalysts (abbreviated as Ag@AgBr). Herein, for the first time, we report a simple and direct microwave-assisted method for the synthesis of monodispersed Ag@AgBr nanocomposites as efficient photocatalysts, which can drive degradation of Rhodamine B (RhB) under visible-light irradiation. By rationally tuning the microwave irradiation time and the content of polyvinylpyrrolidone (PVP) in the precursor solution, we could control the shape, size, and constituents of the Ag@AgBr products. Their strong response towards visible-light is ascribed to the strong SPR effect of metallic Ag components in the nanocomposites. Meanwhile, the as-prepared plasmonic photocatalysts exhibit high activity and durability towards decomposition of RhB. The possible degradation pathways of RhB and a mechanism of the plasmonic photocatalytic process under the visible-light irradiation are proposed.

2. Experimental

2.1. Materials

Silver nitrate (AgNO_3), sodium bromide (NaBr), ethylene glycol (EG), Rhodamine B (RhB), polyvinylpyrrolidone K30 (PVP) and ethanol were purchased from Shanghai Chemical Reagent Co. Ltd. (China). All chemicals in the study were analytical reagent grade and were used without further purification. Deionized water was used in all the experiments. The nitrogen-doped TiO_2 (N- TiO_2) was prepared according to the method reported in the literature [34].

2.2. Preparation of Ag@AgBr photocatalysts

Ag@AgBr photocatalysts were synthesized by a facile and rapid microwave-assisted nonaqueous route. In a typical procedure, 15 mL of EG was cooled to 0°C in an ice bath, then 2 mmol of AgNO_3 was dissolved in it to form a clear solution. In a separate beaker, 2 mmol of NaBr and 3 mmol of PVP were added to 15 mL of EG, followed by sonication at room temperature to form a homogeneous solution, and then was slowly dropped to the AgNO_3 solution under vigorous stirring for 30 min. The resulting mixture was transferred to a 100 mL flask, and the flask was placed into a XH-MC-1 microwave reactor system (XiangHu Science and Technology Equipment Co., Ltd., Beijing, China). The mixture was heated to 160°C by microwave irradiation and kept at the temperature for 10 min. Then the reaction system was quickly cooled to room temperature by an ice bath. The obtained products were collected by centrifugation, washed with absolute ethanol several times, and then dried in vacuum at 45°C for 12 h. The sample was denoted as T-10. In the control experiment, the time series of samples denoted as T-20 and T-30 represent the samples prepared for 20 min and 30 min, respectively, with identical other conditions.

For comparison, AgBr nanoparticles were also prepared by a precipitation method without microwave irradiation. 30 mL of EG was cooled to 0°C in an ice bath, then 4 mmol of AgNO_3 was dissolved in it with magnetic stirring to form a clear solution. In addition, 4 mmol of NaBr and 6 mmol of PVP were dissolved in 30 mL of EG at room temperature to form a homogeneous solution, which then was slowly dropped to the AgNO_3 solution under vigorous stirring for 30 min, resulting in the formation of a primrose yellow dispersion containing AgBr nanoparticles. The obtained products were collected by centrifugation, washed with absolute ethanol several times, and then dried in vacuum at 45°C for 12 h.

2.3. Characterization

The phase of as-synthesized products were characterized using X-ray diffraction (XRD, Shimadzu XRD-6000) with $\text{Cu K}\alpha$

radiation ($\lambda = 1.5406 \text{ \AA}$) at a scanning rate of 4° min^{-1} . The composition, morphology, and size of the products were examined by scanning electron microscopy (SEM, JSM-6480), transmission electron microscopy (TEM, JEOL JEM-2100), energy dispersive X-ray spectroscopy (EDS, attached to SEM), and X-ray photoelectron spectroscopy (XPS, PHI 5000). The photocatalytic activity measurement was conducted on a GHX-2 photochemical reactor (Science and Education equipment Co., Ltd., YangZhou, China) (Fig. S1) with a 500 W of tungsten lamp (Small500WR7S, Philips) as the light source.

2.4. Photocatalytic activity measurement

The photocatalytic activities of the samples were evaluated by the degradation of RhB under visible-light irradiation. A 500 W tungsten lamp with a cutoff filter as the visible-light source ($\lambda > 420 \text{ nm}$) was positioned at ca. 10 cm away from the reaction cell to trigger the photocatalytic reaction. There is a water layer between the reaction system and the lamp to remove the thermal effect of light. The light intensity on the surface of the reaction mixture is ca. 120 mW/cm^2 , estimated with a radiometer (FZ-A, China). The experiments were performed at room temperature as follows: 0.1 g of the photocatalysts was added to 100 mL of RhB solution (10 mg L^{-1} , at natural pH of 5.0) in a Pyrex reactor. Before illumination, the suspensions were stirred at the speed of 1000 rpm in the dark for 30 min to ensure the establishment of an adsorption-desorption equilibrium between the photocatalyst and RhB. The dispersion was then exposed to visible-light irradiation under stirring. At given time intervals, 4 mL of the suspension was pipetted into a centrifuge tube and centrifuged at 8000 rpm for 2 min to remove the remnant photocatalyst. The concentrations of RhB in the supernatant were monitored by checking the absorbance at 553 nm using a UV-2450 (Shimadzu) spectrophotometer. In the recycle experiments, after Ag@AgBr composites were separated from solution, they were washed with ethanol and deionized water before being re-dispersed in the dye solution (100 mL , 10 mg L^{-1}) for another cycle.

2.5. Analytical methods

The final intermediates were conducted by a Agilent gas chromatography interfaced a HED-EM mass spectrometer GC/MS (Agilent 7890A/5975C, USA). The pre-treatment process was as follows: the reacted solution was centrifuged to remove the remnant photocatalyst and the pH was adjusted to 2.0 with 10% HCl. 30 mL of the solution was then extracted with 30 mL dichloromethane for three times and the extracted solution was dehydrated using anhydrous sodium sulphate. Afterward, the dehydrated solution was concentrated to 1 mL. Then, trimethylsilylation was carried out at 50°C for 30 min using 0.5 mL bis(trimethylsilyl) trifluoroacetamide (BSTFA). 1.0 μL of the final sample was injected into GC equipped with DB-5MS column (fused-silica capillary column, $30 \text{ mm} \times 0.25 \text{ mm i.d.}$, $0.25 \mu\text{m}$ film thickness with a 5% equivalent polysilphenylene siloxane) with splitless mode. The temperature program of the column was set as follows: at 60°C , hold time = 1 min, from 60 to 260°C , rate = 10°C/min .

3. Results and discussion

In our study, a direct precipitation reaction between Ag^+ cations and Br^- anions is used to grow monodispersed ball-like AgBr nanoparticles in ethylene glycol with the assistance of polymeric surfactant PVP. It has been widely reported that metal ions could be reduced by ethylene glycol [35]. In the present study, ethylene glycol is proposed to play a key role in the formation of Ag@AgBr.

It acts as a solvent, a microwave-absorber, and a reducing agent in the partial reduction of AgBr to metallic Ag under a moderate temperature.

The phase structure and crystallinity of the as-synthesized Ag@AgBr photocatalysts obtained at different microwave irradiation times were characterized by XRD. As shown in Fig. 1, AgBr phase was detected for all of the Ag@AgBr samples. The XRD peaks at 2θ about 26.8, 31.1, 44.6, 55.4, 64.7 and 73.5° can be indexed to the (1 1 1), (2 0 0), (2 2 0), (2 2 2), (4 0 0) and (4 2 0) crystal planes of AgBr (JCPDS card no. 06-0438), respectively. The result is in good agreement with the XRD patterns of AgBr crystals reported previously [28,32]. No reflections assignable to Ag metal were present in the XRD patterns of samples T-10 and T-20, possibly because the low Ag content was below the detection limit of XRD. However, in the XRD pattern of sample T-30, one additional reflection located at $2\theta = 38.1^\circ$ can be assigned to the (1 1 1) plane of Ag crystal (JCPDS card no. 65-2871), though the diffraction peak was rather weak. This result implies that the content of metal Ag is improved with the increase of microwave irradiation time.

SEM has been used to observe the morphologies of the as-synthesized samples. Typical SEM images of the as-synthesized

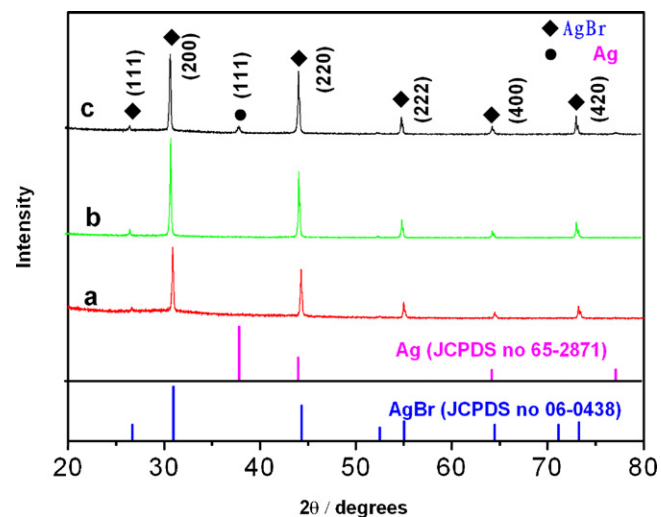


Fig. 1. XRD patterns of the as-prepared Ag@AgBr samples obtained at different microwave irradiation times. (a) 10 min; (b) 20 min; (c) 30 min.

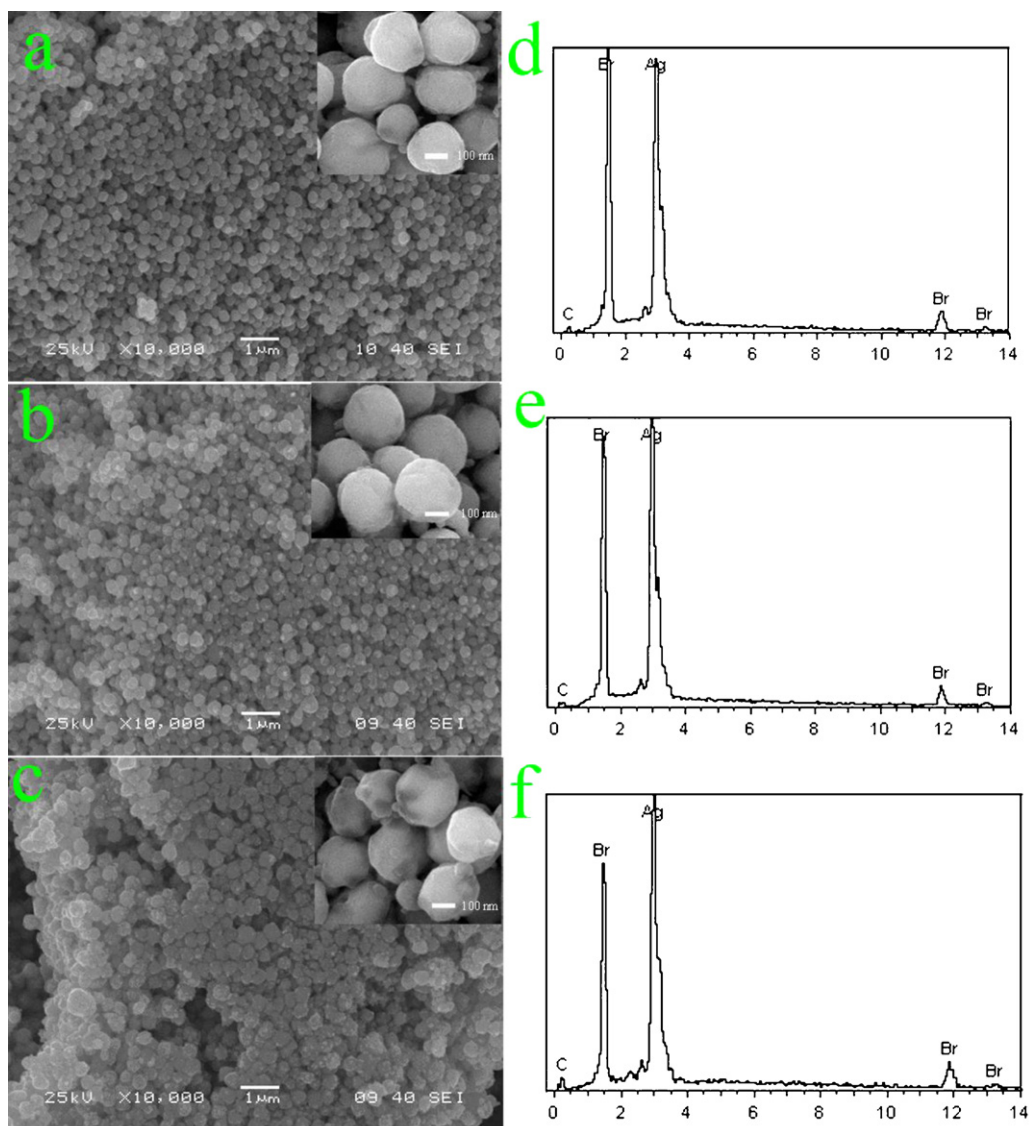


Fig. 2. SEM images and EDS patterns of the as-prepared Ag@AgBr samples obtained with different microwave irradiation times. (a) and (d) 10 min; (b) and (e) 20 min; (c) and (f) 30 min. The insets show the magnified SEM images of the samples.

Ag@AgBr photocatalysts obtained at different microwave irradiation time are shown in Fig. 2. Fig. 2a shows that the sample synthesized in 10 min consists of a large amount of ball-like nanocrystals with an average diameter of 290 nm. As the microwave irradiation time was increased to 20 min, the diameter of AgBr particles was increased to 350 nm, and Ag nanoparticles were distributed uniformly on the surface of AgBr (Fig. 2b). However, when the microwave irradiation time was prolonged to 30 min, the size of the obtained Ag@AgBr particles was increased to around 440 nm, and the morphology became irregular (Fig. 2c). The average diameter of AgBr particles in our experiment is much smaller than the AgBr polyhedra in Zhang's study [30], which may be due to the high viscosity of ethylene glycol in low temperature. The high viscosity of ethylene glycol cause lower diffusion rates of both Ag^+ ions (from AgNO_3) and Br^- ions (from NaBr), and thus the formation of AgBr has a burst nucleation and a lower precipitation rate, which make the AgBr sample have uniform and small size [36]. We also examined the Ag@AgBr samples by TEM. Unfortunately, we failed to obtain exact TEM images of the samples (Fig. S2) because the AgBr nanoparticles were quickly destroyed by the high-energy electron beam during the TEM measurement. Similar phenomena have also been reported by other researchers before [31,37]. EDS has been used to confirm the chemical composition of the as-synthesized samples. The EDS spectra of the Ag@AgBr photocatalysts obtained at different microwave irradiation time are shown in Fig. 2. Carbon element in the EDS spectra comes from the conductive adhesive used as a support for the samples in the SEM measurement. The EDS analysis shows that the sample was composed of Ag and Br elements.

The chemical compositions and surface chemical states of the Ag@AgBr samples were further examined by XPS. The survey spectra of the three Ag@AgBr samples obtained at different microwave irradiation time are similar and confirm Ag and Br as the main components (Fig. 3a). As shown in Fig. 3b, the peaks at 367.5 and 373.3 eV are assigned to those of Ag 3d_{5/2} and Ag 3d_{3/2} binding energies, respectively [38]. These two bands could be further deconvoluted into two peaks, respectively, at 366.8, 368.5 eV and 372.8, 374.5 eV, where the bands at 366.8 and 372.8 eV are attributed to the Ag^+ of AgBr, and those at 368.5 and 374.5 eV are ascribed to the metallic Ag^0 [39–42]. From the XPS peak areas, the surface Ag^0 contents were calculated to be 1.6, 3.9 and 5.7 at% for T-10, T-20 and T-30, respectively, confirming that increasing microwave irradiation time can promote the conversion of AgBr to Ag (Table S1), which is consistent with the XRD results (Fig. 1).

It is found that PVP in the precursor solution also has a significant influence on the size of AgBr nanocrystals. By adjusting the amount of PVP, AgBr with different sizes can be obtained accordingly, and the corresponding SEM images are shown in Fig. 4a–d. For clarity, the samples denoted as PVP-0, PVP-1, PVP-3 and PVP-5 represent the products synthesized with 0 mmol, 1 mmol, 3 mmol and 5 mmol of PVP contents in the precursor solution at 160 °C for 10 min, respectively. The sample synthesized without PVP (PVP-0) takes on a sphere-like morphology with a wide size distribution and an average diameter of about 910 nm (Fig. 4a and e). The addition of PVP can reduce the particle size and improve the size uniformity, as shown in Fig. 4b–d. The sizes of the AgBr nanocrystals are 340, 290, and 260 nm for samples PVP-1, PVP-3, and PVP-5, respectively (Fig. 4f–h). In the reaction system, PVP may serve as a polymeric capping agent, the long polymeric chains of the molecules increase the overall viscosity of the reaction solution to further slow down the precipitation reaction and facilitate the formation of monodisperse-sized AgBr nanoparticles [36].

Fig. 5a shows the photographs of the reaction solution before and after microwave irradiation. The plum color of the colloid after microwave irradiation indicates that some Ag species are formed and embedded in the AgBr matrix. It was reported that plasmonic

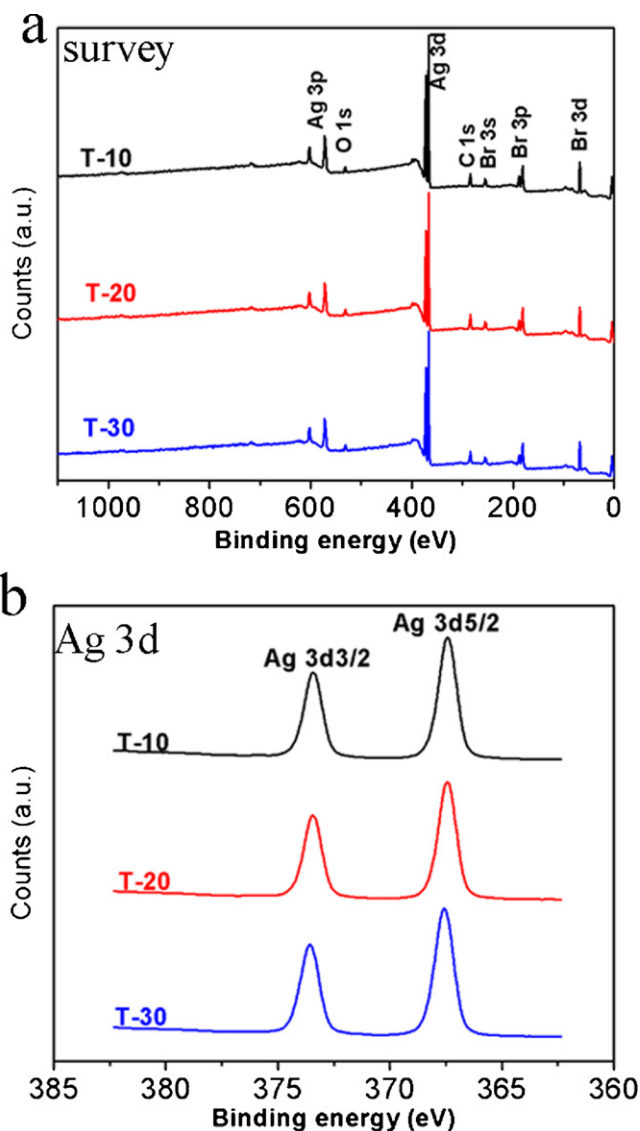


Fig. 3. Typical XPS spectra of the as-prepared Ag@AgBr samples: (a) survey and (b) Ag 3d.

nanostructured metals have a positive effect on the optical absorption of plasmonic-metal-semiconductor composite photocatalysts [33]. The formation of Ag metal on the surface of AgBr can extend and enhance absorption capacity. The existence of Ag metal in the products can be further confirmed by UV/vis diffuse reflectance spectra (UV/vis DRS). As shown in Fig. 5b, the Ag@AgBr nanocrystals exhibit enhanced absorption in the visible-light region in comparison with AgBr nanocrystals. The strong absorption in the region of 450–650 nm should result from the strong SPR of Ag nanoparticles, which is consistent with previous report [33]. Since AgBr is very sensitive to UV light and can be reduced to metal Ag under UV light, it is difficult to obtain the exact UV/vis DRS of pristine AgBr sample.

Although various structures of Ag@AgBr photocatalysts have been prepared by a variety of methods [26,39,41,42], the monodispersed and uniform Ag@AgBr ball-like photocatalysts have not been reported before. Meanwhile, previous study were all focus on the photo-degradation of methyl orange (MO) as a probe reaction, no investigation on the photodegradation of RhB. As a kind of the most commonly used xanthenes dyes in textile industry, RhB has been found to be potentially toxic and carcinogenic and is being widely studied as a representative water pollutant [43].

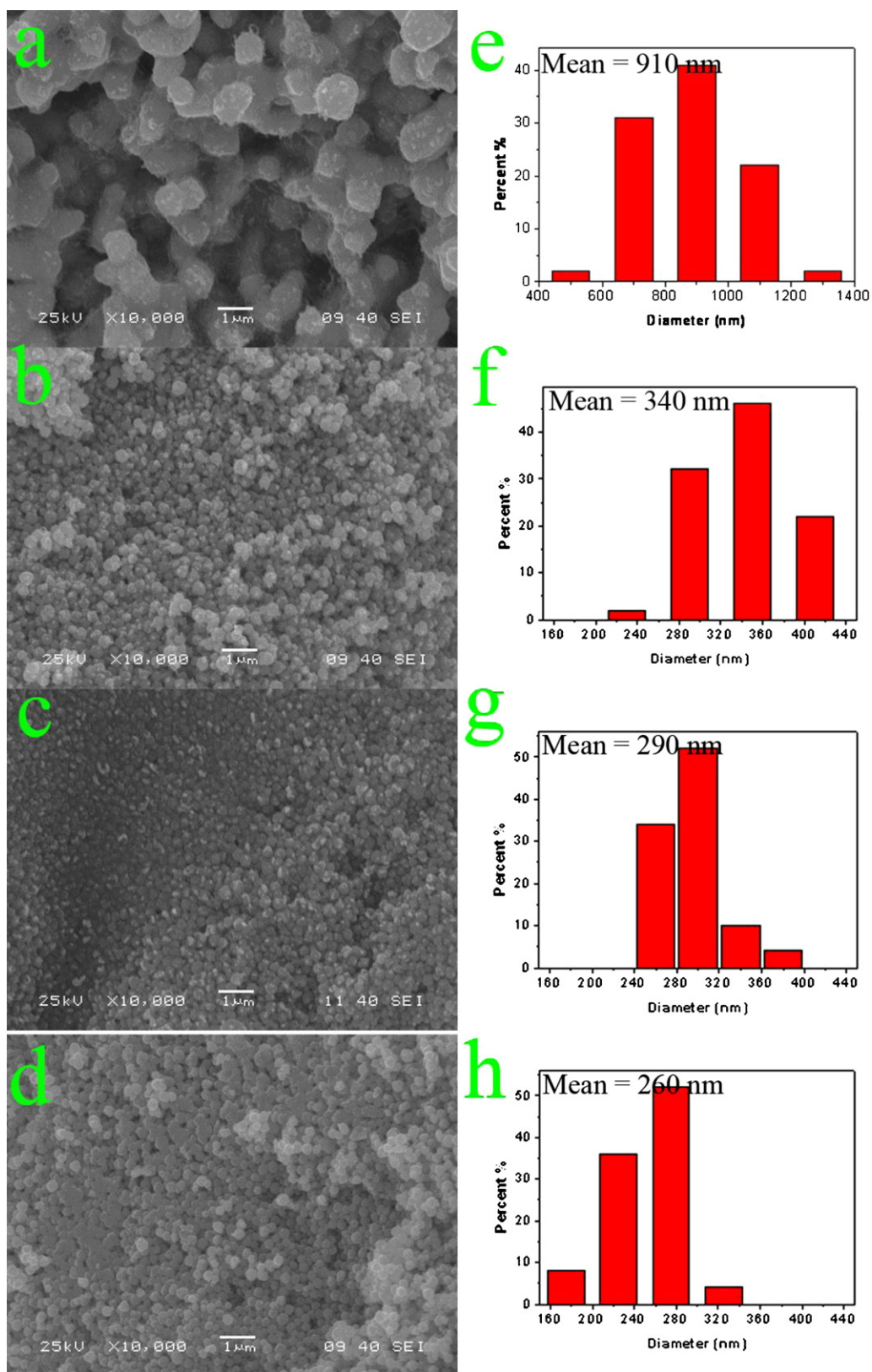


Fig. 4. SEM images and particle size distribution of the as-prepared Ag@AgBr samples obtained under microwave irradiation of 10 min with different PVP contents in the precursor solution. (a) and (e) 0 mmol; (b) and (f) 1 mmol; (c) and (g) 3 mmol; (d) and (h) 5 mmol.

In the present work, the visible-light photocatalytic activity of the Ag@AgBr plasmonic photocatalysts was investigated in terms of photodegradation of RhB in aqueous solution. Fig. 6a displays the temporal evolution of the spectral changes taking place during

the photodegradation of RhB mediated by the typical Ag@AgBr nanocomposites under visible-light irradiation. The sharp decrease in the maximum absorption band implies that RhB molecules suffered a rather cleavage of the whole conjugated chromophore.

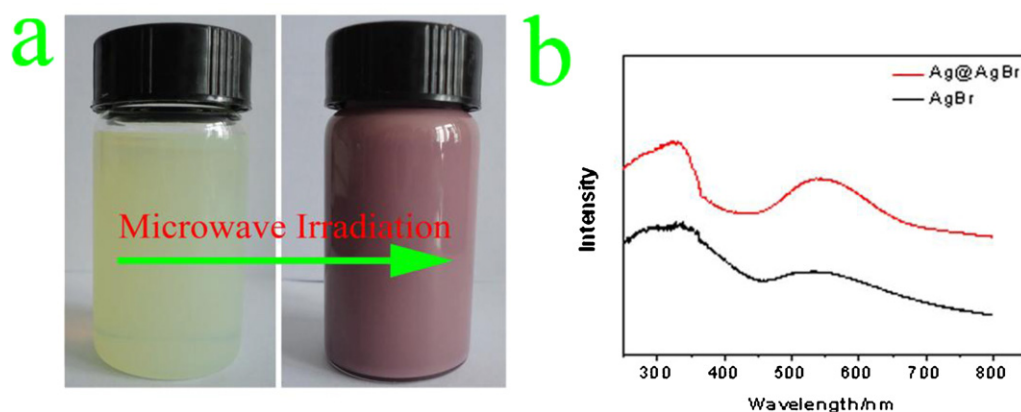


Fig. 5. (a) Photographs of the reaction solution before and after microwave irradiation; (b) UV/vis DRS of Ag@AgBr and AgBr samples.

Furthermore, the absorption maximum of the degraded solution exhibited hypsochromic shifts (Fig. 6b), which is presumed to result from the formation of a series of *N*-de-ethylated intermediates in a stepwise manner. Similar phenomena were also observed in literature and our previous research in $\text{Bi}_2\text{WO}_6\text{-Fe}_3\text{O}_4/\text{RhB}$ system [44]. Nevertheless, hypsochromic shifts of the absorption maximum in our experiment were slight before the complete decomposition. The possible reason is that during visible-light irradiation the *N*-de-ethylation reaction is just a minor process and cycloreversion of RhB is the major process [45]. The color of the dispersion nearly disappeared when the time of visible-light irradiation reached 50 min, indicating the excellent photocatalytic activity and the complete photocatalytic decolorization of RhB aqueous solution during the reaction (insert of Fig. 6a).

The final organic products after photocatalytic reaction were identified by GC/MS. Six benzenoid removal intermediates were identified, including cyclohexanol, cyclohex-1-enol, benzeneacetic acid, 2-phenyl-butylric acid, terephthalic acid and dibutyl phthalate. Besides the intermediates discussed above, some other smaller organic acids such as 2-hydroxy-propionic acid, propane-1,2-diol, hydroxy-acetic acid, butane-1,3-diol, and 4-methyl-pentan-1-ol were also identified by GC/MS (Table 1). On the basis of the above experimental results and the previous studies [44,46], we tentatively propose the possible pathways of degradation of RhB under visible-light illumination as depicted in Fig. 7. Under visible-light irradiation, two pathways occurred during the photoreaction: the *N*-de-ethylation process and the cycloreversion process [47]. On the one hand, the dye is degraded by a series of successive de-ethylation reaction, from *N,N,N',N'*-tetraethylated rhodamine to rhodamine

[45,46]. On the other hand, the conjugated xanthene structure of both RhB and the *N*-de-ethylated intermediates were further degraded into smaller organic molecules during the decolorization process.

The concentration of RhB (*C*) is assumed proportional to the maximum absorbance (*A*) at 553 nm. However, it should be pointed out that since the absorbance may also be contributed by other absorbing components of the intermediates from photodegradation, and thus the concentration determined by UV–vis method should actually be the total concentration of all absorbing components. In this study, we approximately represent the change of RhB concentration (C/C_0) by the variation of absorbance (A/A_0), where *A* is the absorbance at the wavelength of 553 nm during photocatalytic degradation, and A_0 was the absorbance of original RhB solution at 553 nm. To evaluate the photocatalytic activity of Ag@AgBr, we examined the decomposition of RhB in solution over the Ag@AgBr sample under visible-light irradiation as a function of time (Fig. 8). For comparison, we also carried out the decomposition of RhB over AgBr particles and the N-TiO₂ reference photocatalyst under the same reaction condition. It can be seen that the degradation of RhB was extremely slow without photocatalyst under visible-light illumination, and no concentration changes were detected if the experiment was conducted without light irradiation, confirming that the degradation of RhB was caused by photocatalytic reaction. For the Ag@AgBr photocatalysts, the adsorption for RhB is much weaker than that of the AgBr. A possible reason is that the pure AgBr particles have more Br atoms on their surfaces than the Ag@AgBr particles, and thus can provide more RhB adsorption sites because of strong electrostatic interaction

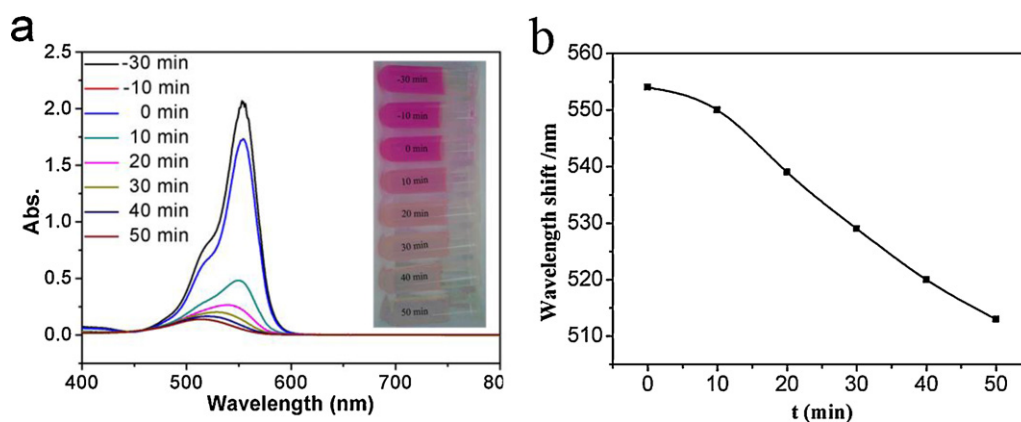
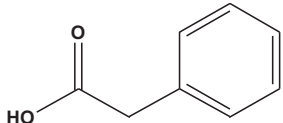
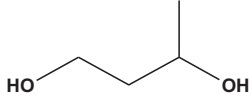
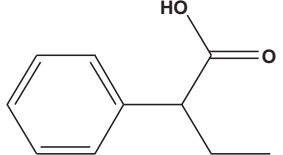
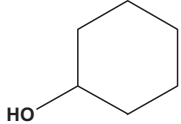
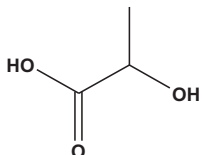
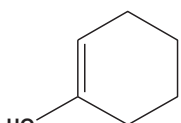
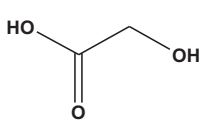
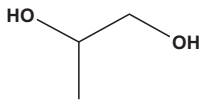
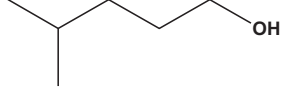
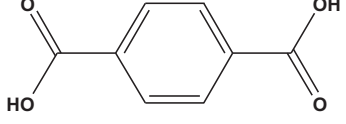
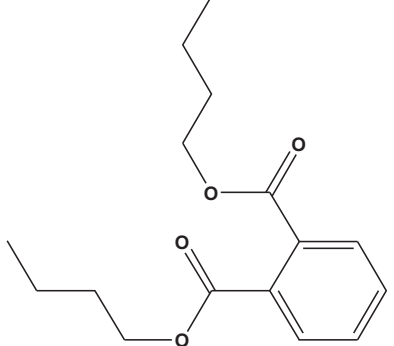


Fig. 6. (a) Temporal UV–vis absorption spectra for RhB solution (10 mg/L, 100 mL, at natural pH of 5.0) in the presence of Ag@AgBr nanocomposite under visible-light irradiation. (b) Wavelength shifts of the absorption peaks as a function of the photocatalytic time.

Table 1
Identification of the degradation intermediates of RhB by GC/MS.

<i>m/z</i>	Retention time	Identified intermediates	Structural formula
136	3.436	Benzeneacetic acid	
90	4.065	Butane-1,3-diol	
164	4.123	2-Phenyl-butyrac acid	
100	4.386	Cyclohexanol	
90	5.153	2-Hydroxy-propionic acid	
98	5.233	Cyclohex-1-enol	
76	5.296	Hydroxy-acetic acid	
76	5.496	Propane-1,2-diol	
102	8.197	4-Methyl-pentan-1-ol	
166	20.156	Terephthalic acid	
278	22.959	Dibutyl phthalate	

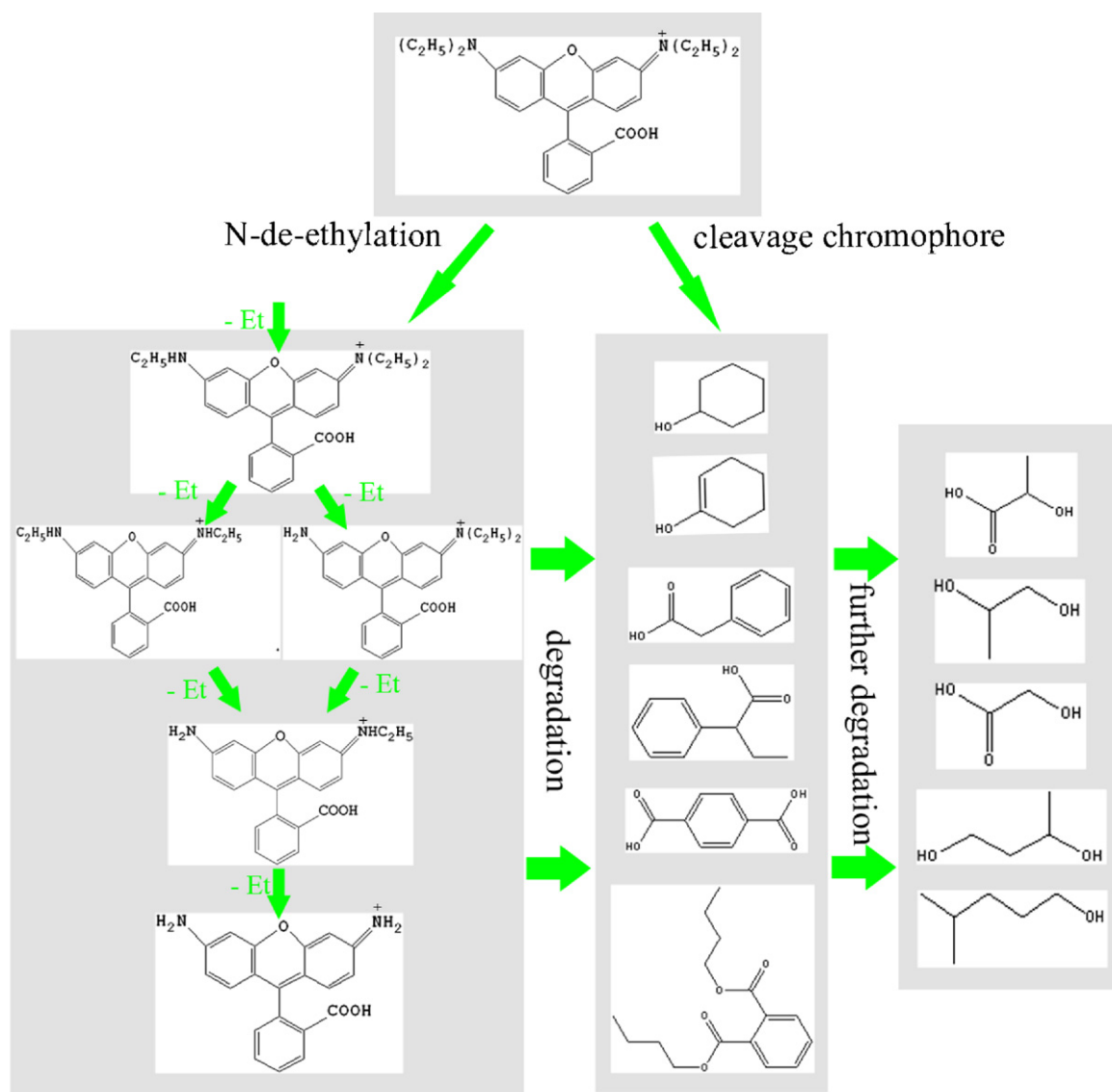


Fig. 7. Proposed degradation pathways for photocatalytic degradation of RhB with Ag@AgBr plasmonic photocatalysts.

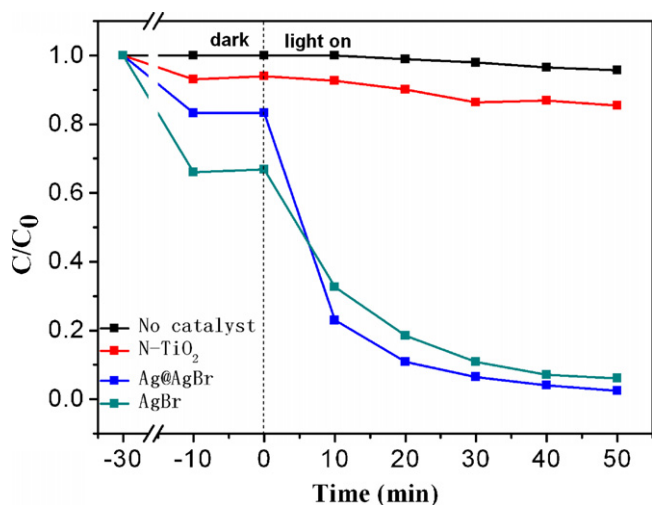


Fig. 8. The photocatalytic degradation efficiencies of RhB as a function of irradiation time over Ag@AgBr nanocomposites and N-TiO₂. The photocatalytic experiments were performed under visible-light illumination, and the initial RhB concentration was 10 mg/L at natural pH of 5.0 in all cases.

between the electron lone pairs of Br atoms and cationic charged RhB molecules. However, it can be found that the Ag@AgBr nanocomposite exhibit higher photocatalytic activities than AgBr and N-TiO₂ during the photocatalytic degradation process.

In order to reveal the relationship between the composition and photodegradation efficiency, the photocatalytic performances of the different Ag@AgBr nanocomposites were investigated at the identical conditions. Fig. 9 shows the degradation of RhB using time series Ag@AgBr samples under visible-light irradiation. Among the time series samples, sample T-30 showed lowest photocatalytic activity than samples T-10 and T-20. The possible reason may be that the increasing microwave irradiation time can enhance the Ag content of the Ag@AgBr nanocomposites, and thus enlarge the interface between Ag and AgBr, which leads to the increasing hole capture by the negative surface charge on the Ag nanoparticles, and reduces the efficiency of charge separation [31]. Moreover, the excessive amounts of Ag can produce photonic shielding effect in the photocatalytic reaction, resulting in photocatalytic performance degradation. The relatively bigger size of T-30 would also decrease its photodegradation efficiency.

Besides the excellent visible-light-driven photocatalytic activity, the renewable photocatalytic activity after photocatalytic

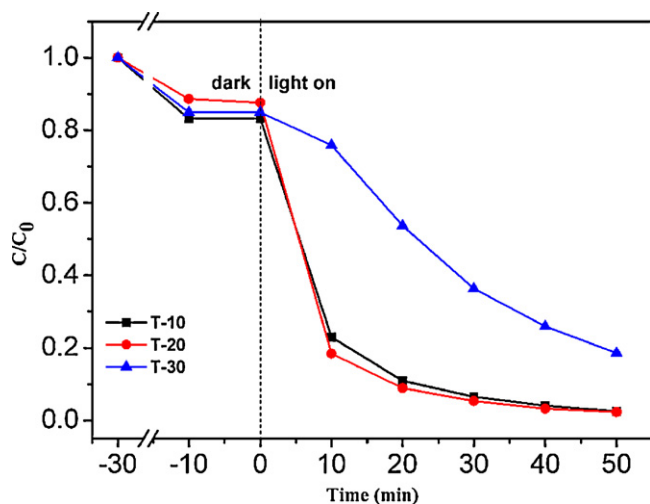


Fig. 9. Visible-light-driven photodegradation curves of RhB over Ag@AgBr photocatalyst obtained with various synthetic time. The photocatalytic experiments were performed under visible-light illumination, and the initial RhB concentration was 10 mg/L at natural pH of 5.0 in all cases.

reactions is also important to the application of a photocatalyst [48]. To evaluate the stability and reusability of Ag@AgBr plasmonic photocatalyst, the circulating runs in the photocatalytic degradation of RhB under visible-light irradiation were also investigated with sample T-10. All the processes and parameters were kept unchanged during the cycling tests. The photocatalytic activity of the Ag@AgBr composites did not show obvious decrease after four catalytic recycles for the photodegradation of RhB (Fig. S3). At the 4th cycle, about 93% of the original RhB was degraded, while it was 98% for the 1st run. These results indicate that photocatalytic activity of Ag@AgBr was highly stable.

The XRD pattern (Fig. S4a) of the Ag@AgBr nanocomposites after recycle experiments exhibits almost identical character to that of the as-prepared sample. The typical SEM images of the Ag@AgBr composites after photocatalytic reaction clearly showed that they keep almost the same morphology as the freshly prepared sample (Fig. S4b). These facts imply that the Ag@AgBr composites are stable during the photocatalytic degradation of the model dye molecules, which is of advantage to their practical applications. Therefore, it is believed that the Ag@AgBr nanocomposite synthesized under our experimental conditions is a highly efficient and stable photocatalyst under visible-light irradiation.

The high photocatalytic activity of the Ag@AgBr plasmonic photocatalysts are mainly attributed to the existence of Ag loaded on the AgBr surface (Fig. 10). Under visible-light illumination, the Ag@AgBr nanocomposite has a strong absorption in the visible-light region due to the SPR effect of Ag nanoparticles, and then a number of electron-hole pairs are generated [22,49]. Because of the synergy of the excellent conductivity of Ag nanoparticles and the polarization field provided by the AgBr, the photogenerated electrons are transferred to the surface of the Ag nanoparticles far from the Ag@AgBr interface and trapped by oxygen molecules (O_2) in the solution to form superoxide ions (O_2^-) and other reactive oxygen species [50], which could also oxidize the RhB dye molecules. At the same time, the photogenerated hole can not only oxidize the RhB dye directly, but can also be transferred to the AgBr surface to oxidize bromine ions (Br^-) to bromine atoms (Br^0), which are also reactive radical species that could oxidize the RhB molecules [32]. On the other hand, besides this plasmonic photocatalytic process, the n-type AgBr semiconductor photocatalysis process simultaneously occurred because AgBr with a small bandgap could also be directly photoexcited under visible-light illumination to

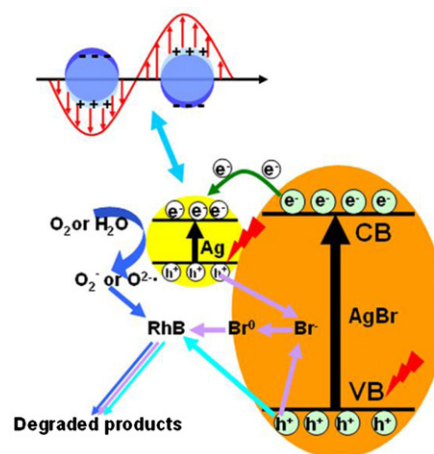


Fig. 10. Schematic illustration of the Ag@AgBr photocatalytic reaction process under visible-light irradiation.

generate electrons in the semiconductor conduction band and holes in the valence band, respectively [30]. Then the electrons can be transferred to the surface of the Ag nanoparticles that together with the injected SPR electrons will initiate the catalytic reaction. In addition, because of the *in situ* production of Ag nanoparticles on the surface of AgBr, the well-defined interface facilitates the interfacial electron transfer and promotes charge carrier separation, which may make another contribution to the high photocatalytic activity [51]. So, the SPR of Ag nanoparticles, the quality of AgBr, and the well-defined interface between Ag and AgBr are assumed to promote the photocatalytic efficiency.

The Ag@AgBr plasmonic photocatalyst is also stable in degrading organic pollutants under visible-light. When subjected to visible light irradiation, Ag@AgBr nanocomposites are excited due to the localized SPR of Ag nanocrystals and generate electron-hole pairs. On the one hand, owing to the excellent conductivity of Ag nanoparticles and the negative charge of the surface of AgBr, the photogenerated electrons could be far from the surface of AgBr and transferred quickly to the present molecular oxygen to form the reactive oxygen species [22]. Thus, an Ag^+ ion inside AgBr could avoid being reduced, which may be one factor for the high stability of the Ag@AgBr composites. On the other hand, though the photogenerated holes could oxidize the Br^- ions inside AgBr into Br^0 atoms, they as reactive radical species could oxidize the RhB dye and hence be reduced to Br^- ions again [32]. This good cycle of bromine may be another factor in the stability of the photocatalyst. In a word, the SPR effect of Ag nanoparticles plays an important role in the high photocatalytic activity and stability of the Ag@AgBr photocatalyst.

4. Conclusions

In summary, we have successfully synthesized Ag@AgBr plasmonic photocatalysts with ball-like morphology through a simple one-step microwave-assisted approach. The shape, size, and composition of the Ag@AgBr nanocomposites were well controlled by tuning the microwave irradiation time and the concentrations of PVP. The as-prepared Ag@AgBr plasmonic photocatalysts show excellent photocatalytic performance under visible light irradiation, which is attributed to the SPR effect of the metallic silver component. Meanwhile, the possible degradation pathways of RhB and a mechanism of the plasmonic photocatalytic process was also proposed. It is believed that the obtained Ag@AgBr plasmonic photocatalyst with high activity and strong durability has potential

applications in the degradation of organic contaminations and environmental cleaning.

Acknowledgement

The authors are grateful for financial support from the National Natural Science Foundation of China (No. 51272094 and No. 51072071).

Appendix A. Supplementary data

Supplementary data associated with this article can be found, in the online version, at <http://dx.doi.org/10.1016/j.apcata.2013.01.035>.

References

- [1] A. Fujishima, K. Honda, *Nature* 238 (1972) 37–38.
- [2] F. Han, V.S.R. Kambala, M. Srinivasan, D. Rajarathnam, R. Naidu, *Appl. Catal. A* 359 (2009) 25–40.
- [3] A. Kudo, Y. Miseki, *Chem. Soc. Rev.* 38 (2009) 253–278.
- [4] O.K. Varghese, M. Paulose, T.J. LaTempa, C.A. Grimes, *Nano Lett.* 9 (2009) 731–737.
- [5] M. Kitano, M. Matsuoka, M. Ueshima, M. Anpo, *Appl. Catal. A* 325 (2007) 1–14.
- [6] S. Yamazaki, N. Fujinaga, K. Araki, *Appl. Catal. A* 210 (2001) 97–102.
- [7] H.G. Yang, C.H. Sun, S.Z. Qiao, J. Zou, G. Liu, S.C. Smith, H.M. Cheng, G.Q. Lu, *Nature* 453 (2008) 638–641.
- [8] X. Zhang, F. Zhang, K.Y. Chan, *Appl. Catal. A* 284 (2005) 193–198.
- [9] X.B. Chen, S.S. Mao, *Chem. Rev.* 107 (2007) 2891–2959.
- [10] R. Sasikala, A.R. Shirole, V. Sudarsan, V.S. Kamble, C. Sudakar, R. Naik, R. Rao, S.R. Bharadwaj, *Appl. Catal. A* 390 (2010) 245–252.
- [11] H.X. Li, Z.F. Bian, J. Zhu, Y.N. Huo, H. Li, Y.F. Lu, *J. Am. Chem. Soc.* 129 (2007) 4538–4539.
- [12] J.C. Yu, L.Z. Zhang, Z. Zheng, J.C. Zhao, *Chem. Mater.* 15 (2003) 2280–2286.
- [13] S.U.M. Khan, M. Al-Shahry, W.B. Ingler, *Science* 297 (2002) 2243–2245.
- [14] R. Asahi, T. Morikawa, T. Ohwaki, K. Aoki, Y. Taga, *Science* 293 (2001) 269–271.
- [15] T. Ohno, T. Mitsui, M. Matsumura, *Chem. Lett.* 32 (2003) 364–365.
- [16] W. Zhao, W.H. Ma, C.C. Chen, J.C. Zhao, Z.G. Shuai, *J. Am. Chem. Soc.* 126 (2004) 4782–4783.
- [17] M.I. Litter, *Appl. Catal. B* 23 (1999) 89–114.
- [18] S.K. Ghosh, T. Pal, *Chem. Rev.* 107 (2007) 4797–4862.
- [19] C. Noguez, *J. Phys. Chem. C* 111 (2007) 3806–3819.
- [20] D.J. Wang, G.L. Xue, Y.Z. Zhen, F. Fu, D.S. Li, J. Mater. Chem. 22 (2012) 4751–4758.
- [21] X. Chen, H.Y. Zhu, J.C. Zhao, Z.F. Zheng, X.P. Gao, *Angew. Chem. Int. Ed.* 47 (2008) 5353–5356.
- [22] P. Wang, B.B. Huang, X.Y. Qin, X.Y. Zhang, Y. Dai, J.Y. Wei, M.H. Whangbo, *Angew. Chem. Int. Ed.* 47 (2008) 7931–7933.
- [23] P. Wang, B.B. Huang, X.Y. Zhang, X.Y. Qin, Y. Dai, Z.Y. Wang, Z.Z. Lou, *Chem-CatChem* 3 (2011) 360–364.
- [24] P. Wang, B.B. Huang, Z.Z. Lou, X.Y. Zhang, X.Y. Qin, Y. Dai, Z.K. Zheng, X.N. Wang, *Chem. Eur. J.* 16 (2010) 538–544.
- [25] P. Wang, B.B. Huang, Q.Q. Zhang, X.Y. Zhang, X.Y. Qin, Y. Dai, J. Zhan, J.X. Yu, H.X. Liu, Z.Z. Lou, *Chem. Eur. J.* 16 (2010) 10042–10047.
- [26] P. Wang, B.B. Huang, X.Y. Zhang, X.Y. Qin, H. Jin, Y. Dai, Z.Y. Wang, J.Y. Wei, J. Zhan, S.Y. Wang, J.P. Wang, M.H. Whangbo, *Chem. Eur. J.* 15 (2009) 1821–1824.
- [27] C.H. An, S. Peng, Y.G. Sun, *Adv. Mater.* 22 (2010) 2570–2574.
- [28] Y.P. Bi, J.H. Ye, *Chem. Eur. J.* 16 (2010) 10327–10331.
- [29] D.L. Chen, S.H. Yoo, Q.S. Huang, G. Ali, S.O. Cho, *Chem. Eur. J.* 18 (2012) 5192–5200.
- [30] J. Jiang, H. Li, L.Z. Zhang, *Chem. Eur. J.* 18 (2012) 6360–6369.
- [31] J. Jiang, L.Z. Zhang, *Chem. Eur. J.* 17 (2011) 3710–3717.
- [32] H. Wang, X.F. Lang, J. Gao, W. Liu, D. Wu, Y.M. Wu, L. Guo, J.H. Li, *Chem. Eur. J.* 18 (2012) 4620–4626.
- [33] Z.C. Wang, J.H. Liu, W. Chen, *Dalton Trans.* 41 (2012) 4866–4870.
- [34] X.F. Wang, S.F. Li, H.G. Yu, J.G. Yu, S.W. Liu, *Chem. Eur. J.* 17 (2011) 7777–7780.
- [35] Y.G. Sun, Y.N. Xia, *Science* 298 (2002) 2176–2179.
- [36] S. Peng, Y.G. Sun, *J. Mater. Chem.* 21 (2011) 11644–11650.
- [37] Y.D. Li, X.F. Duan, Y.T. Qian, L. Yang, H.W. Liao, *J. Colloid Interface Sci.* 209 (1999) 347–349.
- [38] P. Wang, B.B. Huang, X.Y. Qin, X.Y. Zhang, Y. Dai, M.H. Whangbo, *Inorg. Chem.* 48 (2009) 10697–10702.
- [39] L. Kuai, B.Y. Geng, X.T. Chen, Y.Y. Zhao, Y.C. Luo, *Langmuir* 26 (2010) 18723–18727.
- [40] P. Gangopadhyay, R. Kesavamoorthy, S. Bera, P. Magudapathy, K.G.M. Nair, B.K. Panigrahi, S.V. Narasimhan, *Phys. Rev. Lett.* 94 (2005) 47403.
- [41] D.S. Wang, Y.D. Duan, Q.Z. Luo, X.Y. Li, L.L. Bao, *Desalination* 270 (2011) 174–180.
- [42] H. Xu, Y.H. Song, L. Liu, H.M. Li, Y.G. Xu, J.X. Xia, X.Y. Wu, S.W. Zhao, *J. Chem. Technol. Biotechnol.* 87 (2012) 1626–1633.
- [43] J.F. Guo, B. Ma, A.Y. Yin, K.N. Fan, W.L. Dai, *Appl. Catal. B* 101 (2011) 580–586.
- [44] X. Xu, X.P. Shen, G.X. Zhu, L.Q. Jing, X.S. Liu, K.M. Chen, *Chem. Eng. J.* 200–202 (2012) 521–531.
- [45] K. Yu, S.G. Yang, H. He, C. Sun, C.G. Gu, Y.M. Ju, *J. Phys. Chem. A* 113 (2009) 10024–10032.
- [46] Z. He, C. Sun, S.G. Yang, Y.C. Ding, H. He, Z.L. Wang, *J. Hazard. Mater.* 162 (2009) 1477–1486.
- [47] C.C. Chen, X.Z. Li, W.H. Ma, J.C. Zhao, H. Hidaka, N. Serpone, *J. Phys. Chem. B* 106 (2002) 318–324.
- [48] S.K. Li, F.Z. Huang, Y. Wang, Y.H. Shen, L.G. Qiu, A.J. Xie, S.J. Xu, *J. Mater. Chem.* 21 (2011) 7459–7466.
- [49] M.R. Hoffmann, S.T. Martin, W. Choi, D.W. Bahnemann, *Chem. Rev.* 95 (1995) 69–96.
- [50] S.S. Soni, M.J. Henderson, J.F. Bardeau, A. Gibaud, *Adv. Mater.* 20 (2008) 1493–1498.
- [51] L. Han, P. Wang, C.Z. Zhu, Y.M. Zhai, S.J. Dong, *Nanoscale* 3 (2011) 2931–2935.